

Accepted Manuscript

Synthesis, spectroscopic (UV-vis and GIAO NMR), crystallographic and theoretical studies of triazine heterocyclic derivatives

Salman A. Khan, Abdullah Y. Obaid, Laila M. Al-Harbi, Muhammad Nadeem Arshad, Onur Şahin, Cem Cüneyt Ersanlı, R.M. Abdel-Rehman, Abdullah M. Asiri, Michael B. Hursthouse

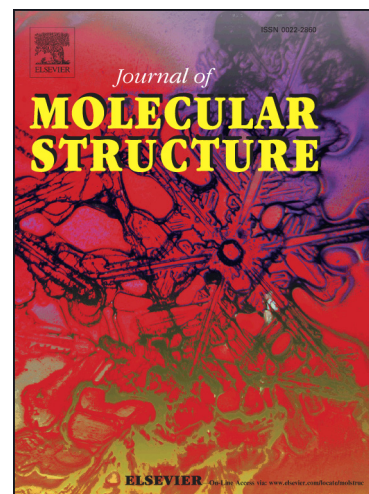
PII: S0022-2860(15)00379-8
DOI: <http://dx.doi.org/10.1016/j.molstruc.2015.04.036>
Reference: MOLSTR 21490

To appear in: *Journal of Molecular Structure*

Received Date: 15 January 2015
Revised Date: 2 March 2015
Accepted Date: 27 April 2015

Please cite this article as: S.A. Khan, A.Y. Obaid, L.M. Al-Harbi, M.N. Arshad, O. Şahin, C.C. Ersanlı, R.M. Abdel-Rehman, A.M. Asiri, M.B. Hursthouse, Synthesis, spectroscopic (UV-vis and GIAO NMR), crystallographic and theoretical studies of triazine heterocyclic derivatives, *Journal of Molecular Structure* (2015), doi: <http://dx.doi.org/10.1016/j.molstruc.2015.04.036>

This is a PDF file of an unedited manuscript that has been accepted for publication. As a service to our customers we are providing this early version of the manuscript. The manuscript will undergo copyediting, typesetting, and review of the resulting proof before it is published in its final form. Please note that during the production process errors may be discovered which could affect the content, and all legal disclaimers that apply to the journal pertain.



Synthesis, spectroscopic (UV-vis and GIAO NMR), crystallographic and theoretical studies of triazine heterocyclic derivatives

Salman A. Khan^{a,*}, Abdullah Y. Obaid^a, Laila M. Al-Harbi^a, Muhammad Nadeem Arshad^{a,b}, Onur Şahin^c, Cem Cüneyt Ersanlı^d, R. M. Abdel-Rehman^a, Abdullah M. Asiri^{a,b} and Michael B. Hursthouse^e

^a*Chemistry Department, Faculty of Science, King Abdulaziz University P.O. Box 80203, Jeddah 21589, Saudi Arabia*

^b*Centre of Excellence for Advanced Materials Research (CEAMR), King Abdulaziz University P.O. Box 80203, Jeddah 21589, Saudi Arabia*

^c*Scientific and Technological Research Application and Research Center, Sinop University, 57010 Sinop, Turkey*

^d*Department of Physics, Faculty of Arts and Sciences, Sinop University, 57010 Sinop, Turkey*

^e*School of Chemistry, University of Southampton, Southampton, SO17 1BJ, UK*

Abstract

This work presents the synthesis and characterization of triazine heterocyclic derivatives. The spectroscopic properties like nuclear magnetic resonance [NMR, (¹H and ¹³C)] were recorded in CDCl₃ solution and Ultraviolet-Visible (UV-vis) absorption spectrums of compounds, 5,6-diphenyl-[1,2,4]triazin-3-ylamine (**1**), (5,6-diphenyl-[1,2,4]triazin-3-yl)-hydrazine (**2**) and 5,6-diphenyl-4H-[1,2,4]triazine-3-thione (**3**), were recorded in the range of 200-800 nm, using chloroform as base solvent. Molecular geometry of compounds with triazine heterocyclic derivative in the ground state have been calculated using the density functional theory (DFT) with 6-31G(d,p) basis set and compared with the X-ray experimental data. The calculated

results show that the optimized geometry can well reproduce the crystal structures. Total static dipole moment (μ), the average linear polarizability (α) and the first hyperpolarizability (β) values of the investigated molecules have been computed using the same methods. The energetic behavior of compounds in solvent media has been examined using B3LYP method with the 6-31G(d,p) basis set by applying the polarizable continuum model (PCM). The total energy of compounds decreases with increasing polarity of the solvent. Frontier molecular orbitals and the molecular electrostatic potential (MEP), $^1\text{H-NMR}$, and $^{13}\text{C-NMR}$ of three triazine derivatives were investigated using theoretical calculations. The linear polarizabilities and first hyperpolarizabilities of the studied molecules indicate that the compounds **1-3** can be used as a good nonlinear optical material (NLO). Isotropic chemical shifts were calculated using the gauge-invariant atomic orbital (GIAO) method. Comparison of the NMR chemical shifts, absorption wavelengths with the experimental values revealed that DFT and time dependent-density functional theory (TD-DFT) method produce generally closer to good results.

Keywords: 1,2,4-Triazine; Crystal structure; DFT; Non-linear optical properties; HOMO-LUMO; MEP

*Corresponding authors: e-mail address: sahmad_phd@yahoo.co.in

1. Introduction

The usefulness of organic ligands with heteroatoms N, O, S is well known. However when these ligands are coordinated with a metal atom, they show a remarkable biological activities like anti-microbial, anti-viral and anti-tumor *etc.* [1-3]. 1,2,4-Triazine derivatives of Pd(II) and Pt(II) show monodentate and bidentate behavior [4] due to their tautomeric and ambidentate nature. Derivatives of triazines were investigated for their antitumor, fungicidal, herbicidal, insecticidal and activities [5]. Wide use of atrazine as herbicidal compounds

resulted in alarming threat for human health as well as environment [6]. Keeping in view the positive and negative aspects of triazine based molecules Larif et al reported a detailed research explaining the biological activities of various derivatives of triazines using DFT and quantitative structure activity relationship (QSAR) studies [7]. We have recently reported the synthesis and spectroscopic studies of 1,2,4-triazine complexes with Ru(II) [8].

In recent years, DFT has been a shooting star in theoretical modeling. The development of better and better exchange-correlation functionals made it possible to calculate many molecular properties with comparable accuracies to traditional correlated *ab initio* methods, with more favorable computational costs [9]. Literature survey revealed that the DFT has a great accuracy in reproducing the experimental values of in geometry, dipole moment, vibrational frequency, *etc* [10-16]. It was noted that the experimental results belong to solid phase and theoretical calculations belong to gas phase. In the solid state, the existence of the crystal field along with the intermolecular interactions have connected the molecules together, which result in the differences of bond parameters between the calculated and experimental values. Despite the differences observed in the geometric parameters, the general agreement is good and the theoretical calculations support the solid state structure.

In this present paper, we report the crystal structures and spectral characterizations of triazine heterocyclic derivatives. Representing the synthesis of triazine derivatives is given in Scheme 1. The properties of the structure geometry, NLO properties, FMO and MEP for compounds **1-3** at the DFT/B3LYP/6-31G(d,p) level were studied for the first time. Besides these, the experimental and calculated values are valuable for providing insight into NMR, UV-vis spectrum and molecular parameters. The results obtained from theoretical calculations and experiments were compared.

2. Experimental and computational method

2.1. Materials and methods

All chemicals used in this study were purchased from Fluka and used without further purification. The melting point was recorded on Stuart scientific SMP3 (Bibby, UK) melting point apparatus and is reported as uncorrected. The $^1\text{H-NMR}$ and $^{13}\text{C-NMR}$ experiments were performed in Bruker-AVANCE-III 600 MHz at 300K. The compounds were dissolved in CDCl_3 . Chemical shifts (δ) were reported in parts per million (ppm) relative to tetramethylsilane (TMS) for $^1\text{H-NMR}$ and $^{13}\text{C-NMR}$ spectra. $^1\text{H-NMR}$ and $^{13}\text{C-NMR}$ spectra were obtained at a base frequency of 150 and 600 MHz, respectively. The UV-vis absorption spectrum of the title molecules were examined in the range 200-800 nm using Spectro UV-VIS double beam PC scanning spectrophotometer UVD-2960 Labomed Inc. The UV patterns are taken from 1.69×10^{-4} molar solution of compound **1**, 6.46×10^{-5} molar solution of compound **2**, and 1.39×10^{-4} molar solution of compound **3**, dissolved in chloroform.

2.2. Synthesis

2.2.1. 5,6-Diphenyl-[1,2,4]triazin-3-ylamine (1)

Benzil (4g, 19.03 mmol) and aminoguanidine bicarbonate (2.58g, 4.76 mmol) in n-butanol (100 ml) was refluxed for four hours. The reaction was monitored through thin layer chromatography (TLC). The mixture was cooled. The solid obtained was filtered off and recrystallized from ethanol to give yellow crystals. [17]

Yield: 4.09g; 85%; m.p. 160 °C; $^1\text{H-NMR}$ shifts (CDCl_3 , δ ppm): 7.30-7.44 (10H, aromatic), 5.53 (2H, s, NH_2); $^{13}\text{C-NMR}$ shifts (CDCl_3 , δ ppm): 161.18, 157.24, 150.78, 136.04, 135.97, 130.37, 129.52, 129.38, 129.24, 128.53, 128.38; **UV-vis** data (nm): $\lambda_{\text{max}} = 345$.

2.2.2. (5,6-Diphenyl-[1,2,4]triazin-3-yl)-hydrazine (2)

A mixture of 5,6-diphenyl-4H-[1,2,4]triazine-3-thione (5g, 18.84 mmol) and hydrazine hydrate (10 ml) in isopropyl alcohol was refluxed for 4-6 h, until no more H_2S evolved. Acetic acid was added drop wise into mixture to remove the excess of hydrazine till neutralization. The mixture was cooled. The solid obtained was filtered off and crystallized from ethanol to give yellowish crystals [18]

Diffraction data of compounds **1-3** were collected on Oxford Diffraction SuperNova (single source at offset) Eos diffractometer equipped with a graphite-monochromatic $\text{CuK}\alpha$ radiation at 296 K. The structures were solved by direct methods using SHELXS-97 and refined by full-matrix least-squares method using SHELXL-97 [19]. All non-hydrogen atom parameters were refined anisotropically and all H atoms except for H atoms bonded nitrogen atoms were refined using a riding model with C-H distances of 0.93 Å. H atoms bonded nitrogen atoms were located in a difference map and refined freely. The following procedures were implemented in our analysis: program used for molecular graphics were as follow: MERCURY programs [20]; supramolecular analyses: PLATON [21]; software used to prepare material for publication: WinGX [22].

Table 1. Crystal data and structure refinement parameters for compounds **1-3**.

Crystal data	1	2	3
Empirical formula	$\text{C}_{15}\text{H}_{12}\text{N}_4$	$\text{C}_{15}\text{H}_{13}\text{N}_5$	$\text{C}_{15}\text{H}_{11}\text{N}_3\text{S}$
Formula weight	248.29	263.30	265.33
Crystal system	monoclinic	monoclinic	monoclinic
Space group	$\text{P}2_1/c$	$\text{P}2_1/c$	$\text{P}2_1/c$
a (Å)	6.2975 (3)	5.7566 (1)	5.8906 (3)
b (Å)	8.3157 (3)	17.2204 (4)	15.2907 (7)
c (Å)	24.9646 (14)	13.6750 (3)	14.6629 (7)
β (°)	99.577 (5)	94.324 (2)	100.100 (5)
V (Å ³)	1289.13 (11)	1351.76 (5)	1300.24 (11)
Z	4	4	4
D_c (g cm ⁻³)	1.279	1.294	1.355
μ (mm ⁻¹)	0.64	0.66	2.11
θ range (°)	3.6-76.8	3.2-76.2	2.9-76.6
Measured refls.	10676	12294	7131
Independent refls.	2682	2822	2730
R_{int}	0.026	0.025	0.023
S	1.05	1.05	1.05
$R1/wR2$	0.042/0.124	0.035/0.102	0.036/0.105
$\rho_{\text{max}}/\rho_{\text{min}}$ (eÅ ⁻³)	0.12/-0.14	0.17/-0.10	0.19/-0.21

2.4. Computational procedures

In computational procedure, Gaussian 03 [23] program package and GaussView visualization program [24] were used for DFT and Hartree-Fock (HF) calculations. Starting geometries of compounds **1-3** were taken from X-ray refinement data. Full geometry optimization of compounds **1-3** in the ground state were performed by using DFT method with Becke's three-parameters hybrid exchange-correlation functional (B3LYP) [25] employing 6-31G(d,p) basis set [26]. As the first step of our DFT calculation for the investigated compounds **1-3**, the initial geometrical configurations taken from their crystallographically obtained geometrical data with no constraint. Thus, the optimized molecular geometry, total molecular energy and dipole moment calculations were obtained from the optimization output by the computational process. Secondly, the average linear polarizability and first hyperpolarizability properties of the compounds were obtained from molecular polarizabilities based on theoretical calculations. Thirdly, in order to evaluate the energetic behavior and dipole moments of compounds **1-3** in solvent media, theoretical calculations in the four different kinds of solvent [benzene, $\epsilon=2.3$; chloroform $\epsilon=4.9$; ethanol, $\epsilon=24.55$; DMSO, $\epsilon=46.7$] have been carried out by using PCM [27-30]. Fourthly, frontier molecular orbitals (FMOs) were performed with B3LYP/6-31G(d,p) the optimized structure. Fifthly, to investigate the reactive sites of the compounds the molecular electrostatic potentials (MEPs) were evaluated using the same method. Sixthly, for NMR calculations, the geometry of the compounds **1-3**, together with that TMS, is fully optimized. ^1H -NMR and ^{13}C -NMR chemical shifts were calculated within the Gauge-including atomic orbital (GIAO) approach [31] applying the DFT and HF methods and the same basis set as used for geometry optimization. After optimization, the ^1H -NMR and ^{13}C -NMR chemical shifts were converted to the TMS scale by subtracting the calculated absolute chemical shielding of TMS ($\delta=\Sigma-\Sigma_0$, where δ is the chemical shift, Σ is the absolute shielding and Σ_0 is the absolute shielding of TMS), with values of 32.02 and 201.35 ppm for HF/6-31G(d,p) and 32.01 and 184.38 ppm

for B3LYP/6-31G(d,p), respectively. In addition, $^1\text{H-NMR}$ and $^{13}\text{C-NMR}$ chemical shifts are calculated by B3LYP/6-31G(d,p) method in chloroform solution. Finally, the electronic properties, such as HOMO-LUMO energies, absorption wavelengths and oscillator strengths calculated using B3LYP method of the TD-DFT, basing on the optimized structure in chloroform and spectra were calculated using the TD-DFT method in gas phase and chloroform solution.

2.5. Supplementary data

Crystallographic data for the structural analysis have been deposited with the Cambridge Crystallographic Data Centre, CCDC 936603 for **1**, 936601 for **2** and 936602 for **3**. Copies of this information may be obtained free of charge from the Director, CCDC 12 Union Road, Cambridge CB2 1EZ, UK. (Fax: +44 1223 336 033 or e-mail: deposit@ccdc.cam.ac.uk).

Table 2. Comparison of experimental and calculated selected bond lengths, angles and dihedral angles for compounds **1-3** (Å, °).

	X-ray			DFT/B3LYP with 6-31G(d,p)		
	1	2	3	1	2	3
<i>Bond lengths (Å)</i>						
C1–N1	1.348 (2)	1.3468 (18)	1.357 (2)	1.352	1.355	1.388
C1–N3	1.3505 (18)	1.3404 (15)	1.365 (2)	1.341	1.338	1.370
C1–N4	1.3427 (18)	1.3478 (17)	-	1.363	1.365	-
C1–S1	-	-	1.6797 (16)	-	-	1.664
N4–N5	-	1.407 (2)	-	-	1.406	-
N1–N2	1.3332 (16)	1.3309 (15)	1.3383 (19)	1.319	1.314	1.332
C3–N3	1.3262 (17)	1.3294 (15)	1.315 (2)	1.335	1.338	1.313
C2–C3	1.4120 (19)	1.4140 (16)	1.447 (2)	1.424	1.421	1.464
C2–N2	1.3320 (18)	1.3356 (14)	1.310 (2)	1.344	1.348	1.314
C2–C4	1.4842 (19)	1.4863 (16)	1.486 (2)	1.486	1.485	1.484
C3–C10	1.4841 (19)	1.4882 (14)	1.479 (2)	1.487	1.486	1.484
<i>Bond angle (°)</i>						
C1–N4–N5	-	123.01 (12)	-	-	122.82	-
<i>Torsion angles (°)</i>						
N2–C2–C4–C9	135.34 (15)	113.86 (14)	57.1 (2)	138.09	138.82	38.83
N3–C3–C10–C11	122.92 (16)	150.42 (13)	-143.30 (17)	140.95	140.29	-144.15

C4–C2–C3–C10	-2.5 (2)	9.9 (2)	-5.9 (2)	-13.82	-14.24	17.07
<i>Dihedral angles (°)</i>						
A/B	43.49(6)	64.04(4)	59.81(5)	40.83	40.21	41.54
A/C	56.74(5)	27.58(6)	34.91(6)	37.00	37.68	33.69
B/C	55.34(4)	65.59(5)	63.85(4)	57.29	57.85	58.67

3. Results and discussion

3.1. Description of the crystal structures

Details of data collection and crystal structure determinations are given in Table 1. Selected bond lengths and angles are collected in Table 2, respectively. The molecular structures of compounds **1-3** with the atom numbering schemes are shown in Fig. 1. The 5- and 6-phenyl substituents of the 1,2,4-triazine ring are inclined to its mean plane with the dihedral angle of 56.74 (5)° and 43.49 (6)° for compound **1**, 27.58 (6)° and 64.04 (4)° for compound **2** and 34.91 (6)° and 59.81 (5)° for compound **3**, respectively. Each 1,2,4-triazine ring is forced by the steric effect of these bulky groups in adjacent positions of the heterocyclic system. These strong steric interaction causing the appearance of the strains in the 1,2,4-triazine ring results in the distortion of its planarity with the displacements of the 1,2,4-triazine atoms from the best plane within 0.0106 Å for compound **1**, 0.0157 Å for compound **2** and 0.0273 Å for compound **3**. In compounds, the C–N distances show no noteworthy features, with values in the range 1.3404 (15)-1.365 (2) Å, which are shorter than the single-bond length of 1.480 Å and longer than the typical C=N distance of 1.280 Å, indicating partial double-bond character and suggesting conjugation in the heterocycle.

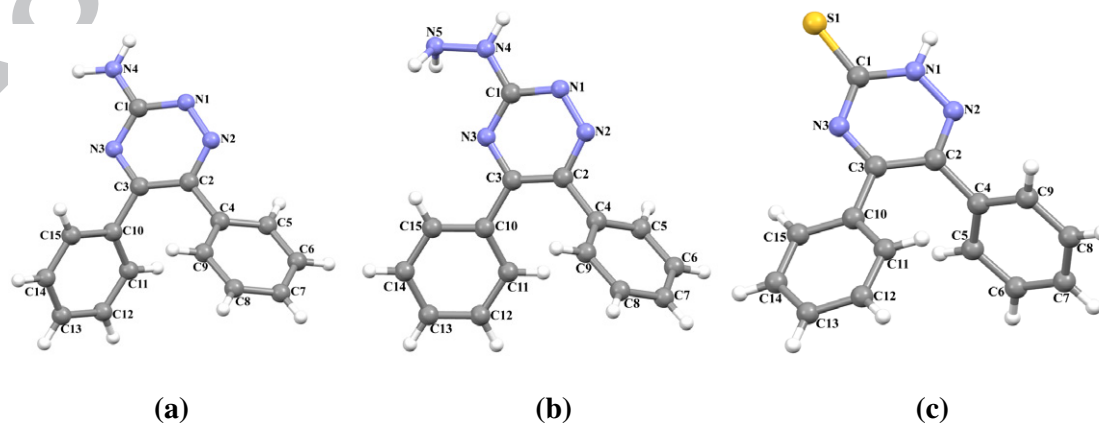


Fig. 1. The molecular structure of compounds **1-3** [(a) for **1**, (b) for **2** and (c) for **3**] showing the atom numbering scheme.

The molecules of compound **1** are linked into sheets by a combination of two N-H...N hydrogen bonds, C-H... π and π ... π interactions are however found absent. Atom N4 in the molecule at (x, y, z) acts as hydrogen-bond donor, *via* atoms H1 and H2, respectively, to atoms N3 at (-x+1, y+1/2, -z+1/2) and N1 at (-x+1, y-1/2, -z+1/2), so forming C(4) [R₂²(8)] chains running parallel to the [010] direction [(Fig. S1) (supplementary material)].

Table 3. Hydrogen-bonds, N-H... π and C-H... π interactions parameters for compounds **1-3** (Å, °).

D-H...A	D-H	H...A	D...A	D-H...A
Compound 1				
N4-H1...N3 ⁱ	0.91	2.48	3.3431 (18)	159
N4-H2...N1 ⁱⁱ	0.97	2.20	3.156 (2)	166
Compound 2				
N4-H4...N1 ⁱ	0.911 (19)	2.095 (19)	3.0019 (17)	173.6 (16)
N5-H5B...N1 ⁱⁱ	0.99 (3)	2.66 (3)	3.508 (3)	143 (2)
N5-H5A...Cg2 ⁱⁱⁱ	0.94 (3)	2.98 (3)	3.759 (2)	140
C13-H13...Cg2 ^{iv}	0.93	2.82	3.6156 (15)	145
Compound 3				
N1-H1...S1 ⁱ	0.98	2.33	3.2862 (14)	163
C14-H14...Cg2 ⁱⁱ	0.93	2.69	3.420 (2)	136

Symmetry codes: (i) -x+1, y+1/2, -z+1/2; (ii) -x+1, y-1/2, -z+1/2 for **1**; (i) -x-1, -y+1, -z; (ii) -x, -y+1, -z; (iii) -x, 1/2+y, 1/2-z; (iv) 1+x, 1/2-y, 1/2+z; Cg2 = C4-C9 for **2**; (i) -x+1, -y+1, -z+2; (ii) x-1, 3/2-y, z-1/2; Cg2 = C4-C9 for **3**.

In compound **2**, amino atom N5 in the reference molecule at (x, y, z) acts as a hydrogen-bond donor, *via* H5B, to atom N1 in the molecule at (-x, -y+1, -z), so forming a centrosymmetric R₂²(10) ring centered at (0, 1/2, 0). Similarly, atom N4 in the molecule at (x, y, z) acts as a hydrogen-bond donor, *via* H4, to atom N1 in the molecule at (-x-1, -y+1, -z), so

forming a centrosymmetric $R_2^2(8)$ ring centered at $(-1/2, 1/2, 0)$. The combination of N-H \cdots N hydrogen bonds generates a chain of edge-fused $R_2^2(8)R_2^2(10)$ rings running parallel to the [100] direction [(Fig. S2) (supplementary material)]. Compound **2** also contain C-H $\cdots\pi$ and N-H $\cdots\pi$ interactions. Details of these interactions are given in Table 3. These C-H $\cdots\pi$ and N-H $\cdots\pi$ interactions play a major role in constructing network [(Fig. S3) (supplementary material)].

The molecules of compound **3** interacts with the protonated nitrogen atom through a N-H \cdots S hydrogen bond forming centrosymmetric $R_2^2(8)$ ring motif with an adjacent cation sulphur atom. In compound **3**, there is also C-H $\cdots\pi$ interaction between C14-H14 and centroid Cg2 (Cg2 = C4-C9). Details of this interaction are given in Table 3. All of these intermolecular interactions give two-dimensional framework results [(Fig. S4) (supplementary material)].

3.2. Optimized geometry and electronic structure

The optimized parameters of compounds **1-3** have been obtained by using the B3LYP/6-31G(d,p) level by DFT method. The computational results for compounds **1-3** were listed together with corresponding X-ray experimental values in Table 2. As seen from Table 2, the optimized bond lengths and the bond angles are slightly different than the X-ray experimental values. We noted here that the experimental results belong to the solid phase and theoretical calculations belong to the gas phase. In the solid state, the existence of a crystal field along with the intermolecular interactions connects the molecules together, which results in the differences in bond parameters between the calculated and experimental values.

According to X-ray and DFT studies, the dihedral angles between the mean planes of A (N1-N3/C1-C3), B (C4-C9) and C (C10-C15) rings for compounds **1-3** are given Table 2.

A logical method for globally comparing the structures obtained with the theoretical calculations (red) is by superimposing the molecular skeleton with that obtained from X-ray diffraction (blue), giving a RMSE of 0.232 Å for compound **1**, 0.226 Å for compound **2** and 0.177 Å for compound **3** (Fig. 2). These differences are due to intermolecular interactions.

These studies indicate that the B3LYP calculation reproduce the geometry of the compounds well.

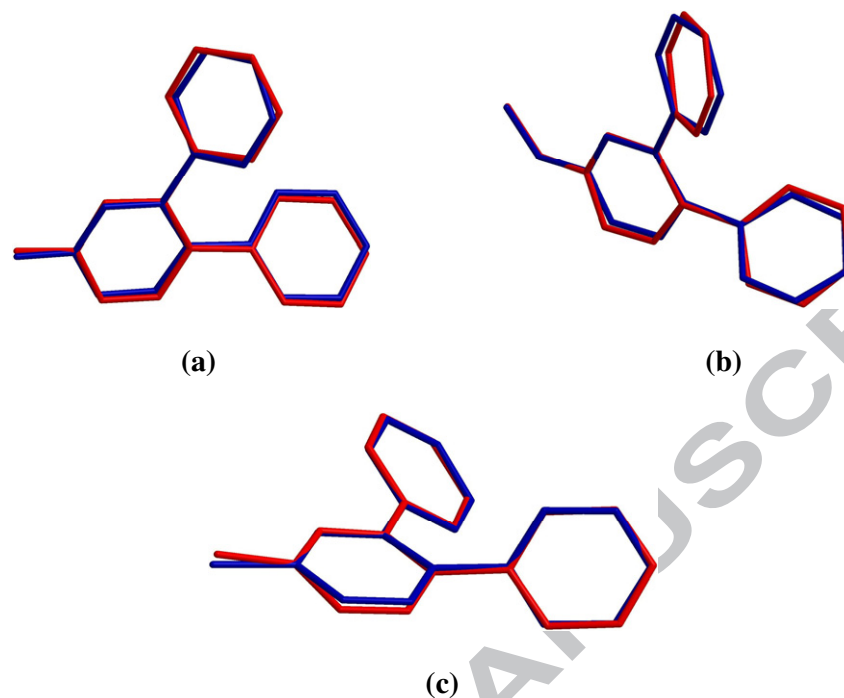


Fig. 2. Atom-by-atom superimposition of the calculated structures (red) over the X-ray structures (blue) for the synthesized compounds **1-3** [(a) for **1**, (b) for **2** and (c) for **3**]. Hydrogen atoms have been omitted for clarity.

3.3. Non-linear optical effects

Non-linear optical (NLO) effects arise from the interactions of electromagnetic fields in various media to produce new fields altered in phase, frequency, amplitude or other propagation characteristics from the incident fields [32]. NLO is at the forefront of current research because of its importance in providing the key functions of frequency shifting, optical modulation, optical switching, optical logic, and optical memory for the emerging technologies in areas such as telecommunications, signal processing, and optical interconnections [33-35]. In order to investigate the relationships among photocurrent generation, molecular structures and NLO, the polarizabilities and hyperpolarizabilities of compounds **1-3** was calculated.

The total static dipole moment (μ), the average linear polarizability (α) and, the first hyperpolarizability (β) can be calculated using the following the Eqs. (1)-(3), respectively [33]. There are x , y and z components:

$$\mu = \sqrt{\mu_x^2 + \mu_y^2 + \mu_z^2} \quad (1)$$

$$\alpha = \frac{\alpha_{xx} + \alpha_{yy} + \alpha_{zz}}{3} \quad (2)$$

$$\beta = \sqrt{(\beta_{xxx} + \beta_{xyy} + \beta_{xzz})^2 + (\beta_{yyy} + \beta_{xxy} + \beta_{yzz})^2 + (\beta_{zzz} + \beta_{xxz} + \beta_{yyz})^2} \quad (3)$$

DFT has been extensively used as an effective method to investigate the organic NLO materials [36]. In order to investigate the NLO properties of structures, μ , α , and β components for compounds **1-3** in gas phase were calculated at the B3LYP/6-31G(d,p) level using polar = ENONLY input to Gaussian 03W program package listed in Table 4. In our present work, the corresponding results of μ , α and β are given directly here, 2.807 D, 27.5889 Å³ and 5.5930x10⁻³⁰ cm⁵/e.s.u. for compound **1**, 4.031 D, 26.2836 Å³ and 3.2817x10⁻³⁰ cm⁵/e.s.u. for compound **2**, and 7.355 D, 28.4596 Å³ and 7.2968x10⁻³⁰ cm⁵/e.s.u. for compound **3**, respectively. Although the calculated values of α and β are smaller than that of (*Z*)-4-methyl-*N*-[2-((2-oxonaphthalen-1(2*H*)-ylidene)methylamino)ethyl]benzenesulfonamide ($\alpha = 39.117$ Å³ and $\beta = 13.011 \times 10^{-30}$ cm⁵/e.s.u. calculated with B3LYP/6-31G(d,p) method) [37] and (*E*)-1-((4-phenoxyphenylimino)methyl)naphthalen-2-olate ($\alpha = 45.34$ Å³ and $\beta = 39.01 \times 10^{-30}$ cm⁵/e.s.u. calculated with B3LYP/6-31G(d,p) method) [38]. Urea is one of the prototypical molecules used in the study of the NLO properties of molecular systems. Therefore it was used frequently as a threshold value for comparative purposes. The calculated values of α and β for compounds **1-3** are, 27.5889 Å³ and 5.5930x10⁻³⁰ cm⁵/e.s.u., 26.2836 Å³ and 3.2817x10⁻³⁰ cm⁵/e.s.u. and 28.4596 Å³ and 7.2968x10⁻³⁰ cm⁵/e.s.u., respectively, which are greater than those of urea (the α and β of urea are 3.831 Å³ and 0.3728x10⁻³⁰ cm⁵/e.s.u. obtained by B3LYP/6-31G(d,p) method). So that, these results indicate that compounds **1-3** are good candidate NLO materials.

Table 4. The calculated static dipole moments (D), linear polarizability (\AA^3) and first hyperpolarizability components (a.u.) for compounds **1-3** in gas phase.

	1	2	3		1	2	3
μ_x	1.3035	3.1918	-2.2562	β_{xxx}	-365.4869	-119.7117	387.5222
μ_y	2.4799	-1.0752	6.7337	β_{xyy}	258.0666	138.4988	-238.1375
μ_z	-0.1726	4.0305	1.9149	β_{yyz}	143.2967	96.8056	-68.3260
				β_{yyy}	-328.0198	-553.2536	560.9760
α_{xx}	35.2489	24.8951	26.7226	β_{xxz}	-31.4658	-152.3444	327.1541
α_{xy}	-2.1673	0.1285	-7.3773	β_{xyz}	7.8488	145.1642	-343.1309
α_{yy}	32.1889	34.8663	38.5578	β_{yyz}	4.6281	71.18243	258.2515
α_{xz}	3.1412	6.5570	4.3371	β_{zzz}	-30.3930	-130.4859	127.3559
α_{yz}	2.7383	-2.2591	5.4078	β_{yzz}	25.2420	112.8170	-196.8959
α_{zz}	15.3292	19.0894	20.0985	β_{zzz}	4.0966	-90.8921	12.0348

3.4. Total energies and dipole moments in solvent media

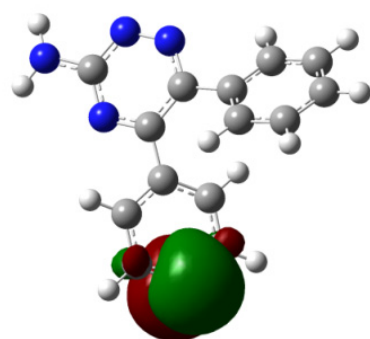
The total energy, energy gap and dipole moment have an effect on the stability of a molecule [39]. We have done optimization in order to evaluate the energetic behavior and dipole moments of the compounds **1-3** in solvent media; we carried out calculations in gas phase and four different kinds of solvent (benzene, chloroform, ethanol and DMSO). The total molecular energies, the highest occupied molecular orbital (HOMO) and the lowest unoccupied molecular orbital (LUMO) energies, dipole moments and chemical hardness (η) have been calculated with the PCM using B3LYP/6-31G(d,p). Results obtained from solvent and gas phase are listed in Table 5. The chemical hardness is quite useful to rationalize the relative stability and reactivity of chemical species. Hard species having large HOMO-LUMO gap will be more stable and less reactive than soft species having small HOMO-LUMO gap [40]. As seen from Table 5, we can infer that the obtained total molecular energies and energy gap (ΔE) between HOMO and LUMO of compounds **1-3** by PCM method and chemical hardness decrease with the increasing polarity of the solvent while the dipole moments rise with the increase of polarity of the solvent for compounds **1-2**. Solvent effects improve the charge delocalized in the molecules, therefore, inducing the dipole moments to be raised. Ground-state dipole moment is an important factor in measuring the solvent effect. A large

ground-state dipole moment gives rise to strong solvent polarity effects [41, 42]. However, we can conclude that the total molecular energies obtained by PCM method decrease with the increasing polarity of the solvent, while the dipole moments and chemical hardness will increase with the increase of the polarity of the solvent for compound **3**. According to these results, the stability of compound **3** increases in going from the gas phase to the solution phase.

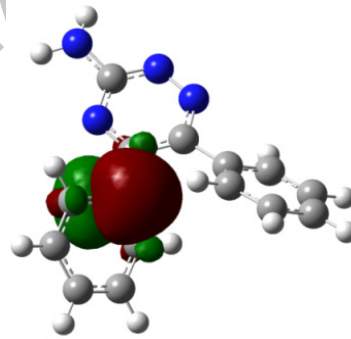
3.5. Frontier molecular orbital energies

Energies HOMO and LUMO are popular quantum mechanical descriptors [43]. According to the investigation on the FMO energy levels of the compounds, which play important roles in interactions between the molecules as well as in electronic spectra of molecule [44], we can find that the corresponding electronic transfer happened between HOMO and LUMO, respectively. The energies of the HOMO are directly related to the ionization potential and characterize the susceptibility of the molecule towards attack of electrophiles. The energy of LUMO is directly related to the electron affinity and characterizes the susceptibility of the molecule attack of nucleophiles. The concept of hard and soft nucleophiles and electrophiles has been also directly related to the relative energies of the HOMO and LUMO orbitals. Hard nucleophiles have a low energy HOMO, soft nucleophiles have a high energy HOMO, hard electrophiles have a high energy LUMO and soft electrophiles have a low energy LUMO. Hard species having large HOMO-LUMO gap will be more stable and less reactive than soft species having small HOMO-LUMO gap [45]. The atomic orbital compositions of the frontier molecular orbitals with energy values, which computed at B3LYP/6-31G(d,p) level for compounds **1-3** in gas phase are shown in Fig. 3. The positive phase is red and the negative one is green. As seen from Fig. 3, in the HOMO: the main electronic transition is occurred at partly phenyl ring and C3 atom, while in LUMO the charge density accumulated at a part of phenyl ring for compound **1**. In compound **2**, it is clear from the figure that while the HOMO is mainly delocalized over the structure, LUMO is delocalized on the whole structure other than hydrazinly group and phenyl ring. In the

HOMO, the charge density is mainly localized on C atom of triazine group and S atom attached to triazine group of molecule for compound **3**. However, in case of the LUMO, more charge density moves to the triazine ring part and S1 atom. Both the HOMO and LUMO are mostly the π -antibonding type orbitals for compounds **1-3**. As can be seen from Table 5, the magnitude of the energy separations between the HOMO and LUMO (transition from HOMO to LUMO) are 6.232, 4.187 and 3.211 eV for compounds **1**, **2** and **3**, respectively, in gas phase. In our present study compound **3** with low chemical hardness 1.6055 eV compared with other compound **1-2** have a low energy gap. Normally, the inhibitor with the least value of chemical hardness is expected to have the highest inhibition efficiency [46]. These large HOMO-LUMO gaps automatically mean high excitation energies for many of excited states, a good stability and a high chemical hardness for the compounds **1-3**.

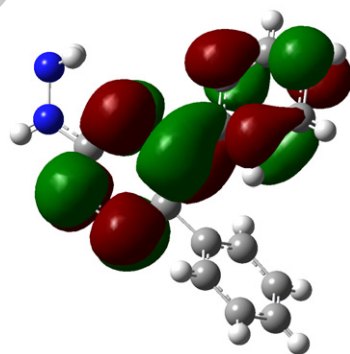


LUMO (-0.262 eV)

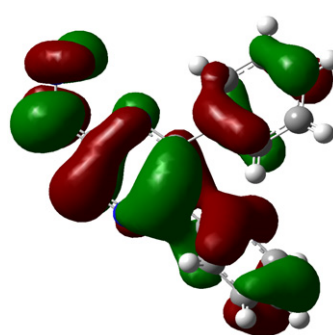


HOMO (-6.494 eV)

(a)

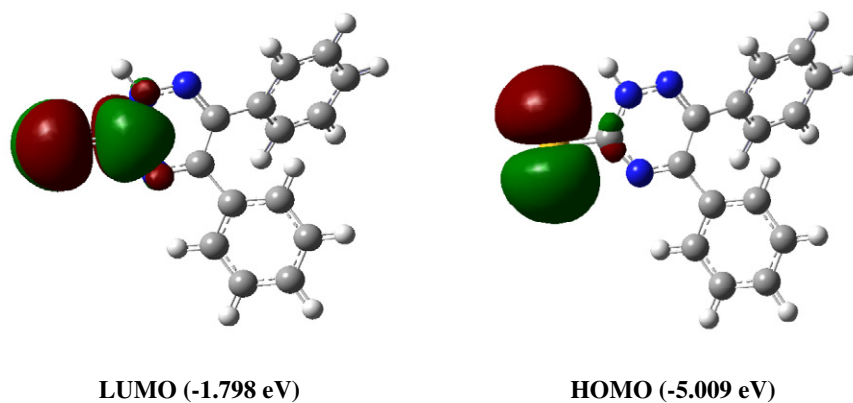


LUMO (-1.931 eV)



HOMO (-6.118 eV)

(b)



(c)

Fig. 3. Molecular orbital surfaces and energy levels given in parentheses for the HOMO and LUMO synthesized compounds **1-3** [(a) for **1**, (b) for **2** and (c) for **3**] computed at B3LYP/6-31G(d,p) level.

Table 5. Calculated energies, frontier orbital energies, chemical hardness and dipole moments of structures for four different solvents.

	Gas phase ($\epsilon = 1$)			Benzene ($\epsilon = 2.3$)			Chloroform ($\epsilon = 4.9$)		
	1	2	3	1	2	3	1	2	3
E_{total} (Hartree)	-797.8311	-852.8783	-1140.4349	-797.8396	-853.1576	-1140.6669	-797.8459	-853.1643	-1140.6749
E_{HOMO} (eV)	-6.494	-6.118	-5.009	-5.892	-5.890	-5.926	-5.927	-5.903	-6.076
E_{LUMO} (eV)	-0.262	-1.931	-1.798	-1.765	-1.860	-2.634	-1.809	-1.887	-2.656
ΔE (eV)	6.232	4.187	3.211	4.127	4.030	3.292	4.118	4.016	3.420
η (eV)	3.1160	2.0935	1.6055	2.0635	2.0150	1.6460	2.0590	2.0080	1.7100
μ (D)	2.807	4.031	7.355	3.330	4.044	8.277	3.712	4.495	9.450
	Ethanol ($\epsilon = 24.55$)			DMSO ($\epsilon = 46.7$)					
	1	2	3	1	2	3			
E_{total} (Hartree)	-797.8520	-853.1707	-1140.6827	-797.8526	-853.1714	-1140.6837			
E_{HOMO} (eV)	-5.971	-5.874	-6.192	-5.974	-5.892	-6.203			
E_{LUMO} (eV)	-1.854	-1.865	-2.679	-1.858	-1.891	-2.680			
ΔE (eV)	4.117	4.009	3.513	4.116	4.001	3.523			
η (eV)	2.0585	2.0045	1.7565	2.0580	2.0005	1.7615			
μ (D)	4.088	4.768	10.550	4.132	4.834	10.693			

3.6. Molecular electrostatic potential

The molecular electrostatic potential (MEP) $V(\mathbf{r})$, is related to the electronic density and is a very useful descriptor in determining the sites for electrophilic and nucleophilic reactions as well as hydrogen bonding interactions [47, 48]. Being a real physical property, $V(\mathbf{r})$ can be determined experimentally by diffraction or by computational methods [44]. MEP maps of the compounds **1-3** were calculated by using the geometry obtained from DFT method at the B3LYP/6-31G(d,p). The negative (red and yellow) and the positive (blue) regions in the MEP were related to electrophilic reactivity and nucleophilic reactivity, respectively (Fig. 4). As can be seen from the Fig. 4, In compounds **1-3**, negative electrostatic potential regions (red color) are mainly localized over 1,2,4-triazine ring atoms. In such a way that, the most negative regions are on the N2 and N1 atoms in compounds **1-2** and $V(\mathbf{r})$ values are -0.058 and -0.056 a.u. for compound **1**, -0.059 and -0.057 a.u. for compound **2**. In compound **3**, the negative $V(\mathbf{r})$ values are -0.060 and -0.058 a.u. S1 and N3 atoms, respectively, which is the most negative regions. However, for the possible nucleophilic reactions, the most positive regions (blue color) in MEP maps are on the hydrogen atoms bonded to N4 for compound **1** and N4 and N5 for compound **2**. The maximum positive regions are located on the H1 and H2 atoms bonded to N4 with $V(\mathbf{r})$ values of 0.041 and 0.046 a.u. for compound **1**, the latter positive sites are localized over the H4 and H5A hydrogen atoms bonded to N4 and N5 atoms with values of 0.032 and 0.042 a.u. for compound **2**, respectively. In compound **3**, a maximum positive region is associated with the N1-H1 bond indicating a possible site for nucleophilic attack with maximum value of 0.048 a.u. In regard to these calculated results, the MEP map indicates that the negative potential sites are on nitrogen atoms as the positive potential sites are around the hydrogen atoms. These regions give knowledge about intermolecular interactions.

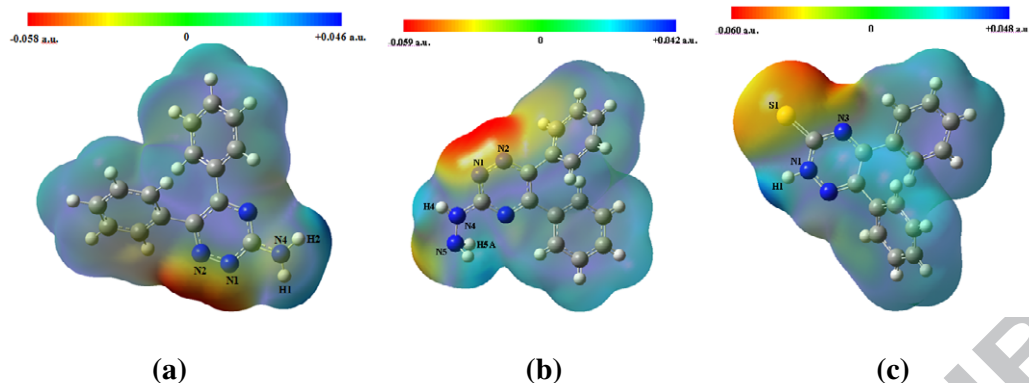


Fig. 4. Molecular electrostatic potential maps of the synthesized compounds **1-3** [(a) for **1**, (b) for **2** and (c) for **3**] calculated at B3LYP/6-31G(d,p) level.

3.7. NMR analysis

The isotropic chemical shifts are frequently used as an aid in identification of reactive organic as well as ionic species. It is recognized that accurate predictions of molecular geometries are essential for reliable calculations of magnetic properties [49]. Therefore, full geometry optimization of compounds **1-3** were performed by using the HF and B3LYP methods with 6-31G(d,p) basis set. Then, GIAO ^1H and ^{13}C chemical shift calculations of the compounds **1-3** have been by the same methods. The ^1H -NMR and ^{13}C -NMR chemical shifts were measured in gas phase and a less polar (CDCl_3) solvent. The results obtained *via* experimental (in chloroform) and theoretical calculations (in gas phase and chloroform) are tabulated in Table 6. The molecule **1** contains twelve protons, out of these, 10 are aromatic and two are amino. There is very clear sharp singlet peak at 5.53 ppm with the intensity of two protons representing the protons (H_1 & H_2) of amino group. The corresponding values we obtained through HF & B3LYP method are 4.30-4.59 & 5.01-5.46, respectively. Since, we had one dimensional proton spectrum so it is difficult to assign separate value for each aromatic proton in experimental results. We have provided aromatic range for all three molecules and these are well comparable with data obtained through theoretical calculations. Similarly for molecule two there are two singlet's appear at 6.64 and 4.18 ppm with the intensity of one and two protons which help us to identify NH & NH_2 protons. The third molecule had one N-

H proton which gave a broad peak at 11.78 ppm the corresponding HF and B3LYP values are 11.62 & 11.36 ppm. ^{13}C -NMR data also gave very good characterization of all three molecules, triazine ring in each molecule contain three carbon atoms C1, C2 & C3. C1 lies between two carbon atoms and it appears at 161.18 ppm, the calculated theoretical values for this signal are 159.23 & 148.23 ppm in CDCl_3 through HF and B3LYP methods for molecule 1. Similarly in 2nd and 3rd molecule this signal appears at 162.20 & 179.24 ppm. The variation in 3rd molecule represents its different environment with other two molecules. The overall assignments for triazine and aromatic carbon atoms are given in Table 6.

Table 6. Experimental and theoretical ^1H -NMR and ^{13}C -NMR isotropic chemical shifts (with respect to TMS, all values in ppm) of compounds 1-3 in gas phase and chloroform.

Compound 1													
Atom	Exp.	HF			B3LYP		Atom	Exp.	HF			B3LYP	
		CDCl_3	CDCl_3	Gas	CDCl_3	Gas			CDCl_3	CDCl_3	Gas	CDCl_3	Gas
H1	5.53	4.59	4.12	5.46	4.93	C1	161.18	159.23	158.16	148.23	147.02		
H2	5.53	4.30	3.70	5.01	4.36	C2	150.78	148.17	147.87	142.40	142.37		
H5	7.30	8.1	7.13	8.70	8.70	C3	157.24	163.31	161.03	145.52	143.60		
H6		7.72	7.37	8.03	7.83	C4	135.97	134.95	135.58	126.19	126.55		
H7		7.55	7.69	7.84	7.61	C5	128.38	128.30	128.77	116.50	127.18		
H8	to	7.25	7.78	7.61	7.49	C6	129.24	126.19	126.06	116.45	116.27		
H9		6.86	8.33	7.37	7.26	C7	128.53	126.04	125.39	115.50	114.96		
H11		7.04	7.35	7.60	7.54	C8	129.24	124.57	124.20	114.74	114.28		
H12		7.24	7.23	7.60	7.37	C9	129.38	128.41	128.38	117.47	117.49		
H13		7.68	7.82	7.94	7.67	C10	136.04	132.73	133.58	125.56	126.23		
H14		7.72	7.79	8.06	7.81	C11	128.38	129.40	129.45	118.38	118.41		
H15	7.44	8.26	9.06	8.70	8.60	C12	129.52	123.76	123.57	114.60	114.21		
						C13	130.37	129.30	128.22	118.14	117.12		
						C14	129.52	125.38	126.05	126.39	115.95		
						C15	128.38	129.14	129.02	118.38	118.58		

Compound 2													
Atom	Exp.	HF			B3LYP		Atom	Exp.	HF			B3LYP	
		CDCl_3	CDCl_3	Gas	CDCl_3	Gas			CDCl_3	CDCl_3	Gas	CDCl_3	Gas
H4	6.64	6.49	5.97	6.93	6.38	C1	162.20	168.20	167.28		151.22		
H5A	4.18	3.69	3.38	3.79	3.53	C2	151.21	153.78	153.40		141.84		

H5B	4.18	3.67	3.26	3.73	3.35	C3	157.12	164.47	161.94	144.98
H5	7.31	8.82	8.78	8.76	8.76	C4	128.62	137.01	137.36	126.07
H6		8.01	7.78	8.03	7.84	C5	128.38	130.09	130.76	116.48
H7		7.82	7.56	7.82	7.59	C6	129.25	128.89	128.83	116.39
H8		7.55	7.29	7.60	7.48	C7	135.92	128.91	128.44	115.56
H9	to	7.29	7.14	7.38	7.25	C8	129.25	127.36	126.95	114.79
H11		7.60	7.54	7.63	7.58	C9	128.38	131.18	131.15	117.39
H12		7.55	7.30	7.62	7.40	C10	130.52	134.51	135.37	125.86
H13		8.04	7.73	7.96	7.40	C11	128.39	133.44	133.47	118.36
H14		8.03	7.76	8.06	7.69	C12	129.56	126.22	126.12	124.74
H15	7.49	8.91	8.75	8.71	8.58	C13	135.96	133.39	132.26	118.20
						C14	129.56	127.79	127.53	116.43
						C15	128.39	133.08	132.93	118.42

Compound 3

Atom	Exp.	HF		B3LYP		Atom	Exp.	HF		B3LYP	
		CDCl ₃	Gas	CDCl ₃	Gas			CDCl ₃	Gas	CDCl ₃	Gas
H1	11.78	11.62	10.65	11.36	10.59	C1	179.24	199.94	187.15	170.18	169.63
H5	7.27	7.35	7.13	7.42	7.22	C2	146.66	150.76	148.38	136.14	133.87
H6		7.63	7.37	7.69	7.44	C3	160.73	169.81	167.77	148.64	147.26
H7		8.00	7.69	7.94	7.67	C4	130.28	133.07	134.05	122.78	123.45
H8		8.04	7.78	8.05	7.81	C5	128.39	131.76	131.34	117.29	116.89
H9	to	8.54	8.33	8.37	8.19	C6	128.74	127.44	127.23	115.32	114.82
H11		7.54	7.35	7.60	7.45	C7	129.40	131.77	130.56	117.62	116.47
H12		7.53	7.23	7.62	7.46	C8	128.74	128.95	128.85	116.96	116.54
H13		8.17	7.82	8.03	7.74	C9	128.39	129.79	129.48	115.84	115.60
H14		8.05	7.79	8.07	7.83	C10	132.22	131.48	132.46	123.49	124.15
H15	7.57	9.15	9.06	8.80	8.71	C11	128.60	134.41	133.69	118.86	118.31
						C12	130.10	125.42	124.90	114.72	113.94
						C13	129.86	136.41	134.74	120.62	119.14
						C14	130.10	127.65	127.59	116.92	116.51
						C15	128.39	135.11	135.27	119.75	119.94

3.8. Electronic absorption spectra

In order to understand electronic transitions, electronic absorption spectra was calculated with TD-DFT method, based on the B3LYP/6-31G(d,p) level optimized structure of compounds **1-3**. TD-DFT calculations of compounds **1-3** in gas phase and chloroform solvent were performed by using PCM model. The experimental and computed electronic values, such as

absorption maxima of λ (which is a function of the electron availability) and Singlet A values (which are from CI expansion coefficients are used to calculate the percentage contribution of the translations), excitation energies (E), and oscillator strengths (f) are reported Table S1 (supplementary material). The major contributions of the transitions were designated with the aid of SWizard program [50]. The electronic absorption spectra of the investigated compounds show an electronic absorption band with maxima at 345, 355 and 440 nm for compound **1**, **2** and **3**, respectively, these values are very close to calculated absorption peak. These experimental bands at 345, 355 and 440 nm for compounds **1-3**, respectively are attributed mainly to a HOMO→LUMO transitions are predicted as $\pi\rightarrow\pi^*$ transitions. The other wavelength, excitation energies, oscillator strengths and calculated counterparts with major contributions in gas phase and solvent can be seen in Table S1 (supplementary material).

4. Conclusions

In this paper, we have synthesized compounds [$C_{15}H_{12}N_4$ (**1**), $C_{15}H_{13}N_5$ (**2**) and $C_{15}H_{11}N_3S$ (**3**)] including triazine heterocyclic derivative, and characterized it using structural (XRD) technique. The optimized parameters of compounds **1-3** have been obtained by using the B3LYP/6-31G(d,p) level by DFT method. The X-ray structure is found to be very slightly different from its optimized counterparts. It is noted here that the experimental results are for the solid phase and the theoretical calculations are for the gas phase. In the solid state, the existence of the crystal field together with the intermolecular interactions holds the molecules together, which results in differences between X-ray experimental and calculated values for the bond parameters. In spite of the differences observed in the geometric parameters, the common agreement is good and the theoretical calculations support the solid-state structures. Furthermore, the non-linear optical properties: total static dipole moment and the first hyperpolarizability properties of compounds have been calculated in order to get insight into compounds. And also the value of the ΔE explains the eventual charge transfer interaction

taking place within the molecule of compounds. The total energy of molecules decreases with the increasing polarity of the solvent for compounds **1-3**. Chemical hardness decrease with the increasing polarity of the solvent while the dipole moments rise with the increase of polarity of the solvent for compounds **1-2**. However, dipole moments and chemical hardness have been increased with the increase of the polarity of the solvent for compound **3**. According to these results, the stability of compound **3** increases in going from the gas phase to the solution phase. To predict reactive sites for electrophilic and nucleophilic attack for the investigated molecules, MEP studies were carried out. Thus, it would be predicted that the nitrogen atoms will be the most reactive site for electrophilic attack and hydrogen atoms will be the reactive site for nucleophilic attack. These sites give information about the possible areas for inter- and intramolecular hydrogen bonds. The magnetic properties of the compounds **1-3** were observed and calculated. The theoretical $^1\text{H-NMR}$ and $^{13}\text{C-NMR}$ chemical shift results of compounds **1-3** are generally are closer to the experimental $^1\text{H-NMR}$ and $^{13}\text{C-NMR}$ shift data. The electronic properties were also experimental and calculated electronic spectrum was recorded with help of UV-vis spectrometer. The experimental bands at 345, 355 and 440 nm for compounds **1-3**, respectively are attributed mainly to a HOMO \rightarrow LUMO transitions are predicted as $\pi\rightarrow\pi^*$ transitions. The comparisons of the predicted bands with the experimental bands were done and show an acceptable general agreement. The present quantum chemical study may further play an important role in understanding of dynamics of these molecules.

In summary, very complete characterizations of studied novel compounds were given in the present paper. We hope the results of this study will be helpful for the design and synthesis new materials.

5. Acknowledgment

This paper was funded by the Deanship of Scientific Research (DSR), King Abdulaziz University, under grant No. (50-3-1432/HiCi). The authors, therefore, acknowledge with thanks DSR technical and financial support.

References

- [1] S.B. Padhye, G.B. Kaufman, *Coord. Chem. Rev.* 63 (1985) 127-160.
- [2] A.M. Asiri, S.A. Khan, *Molecules* 15 (2010) 4784-4791.
- [3] E. Bermejo, R. Carballo, A. Castineiras, R. Dominguez, C.M. Mossemer, J. Strahle, D.X. West, *Polyhedron* 18 (1999) 3695-3702.
- [4] M. Ghassemzadeh, M. Mirza-Aghayan, B. Neumüller, *Inorg. Chim. Acta* 358 (2005) 2057-2065.
- [5] C. Lee, S. Lo, J. Lim, V.C.P. da-Costa, S. Ramezani, O.K. Oz, G.M. Pavan, O. Annunziata, X. Sun, E.E. Simanek, *Mol. Pharmaceutics*, 10 (2013) 4452-4461
- [6] J.N. Hogarth, N. Seike, Y. Kobara, A. Habib, J.J. Namd, J.S. Lee, Qilu Li, X. Liu, Li Jun, G. Zhang, S. Masunaga, *Chemosphere* 86 (2012) 718-726.
- [7] M. Larif, A. Adad, R. Hmammouchi, A.I. Taghki, A. Soulaymani, A. Elmidaoui, M. Bouachrine, T. Lakhlifi, *Arabian Journal of Chemistry*
<http://dx.doi.org/10.1016/j.arabjc.2012.12.033>.
- [8] A.M. Asiri, A.O. Baghlaf, R.M. Abdel-Rahman, S.A. Khan, M. Ishaq *Asian J. Chem.* 25 (2013) 7779-7782.
- [9] F.D. Proft, P. Geerlings, *Chem. Rev.* 101 (2001) 1451-1464.
- [10] G. Fitzgerald, J. Andzelm, *J. Phys. Chem.* 95 (1991) 10531-10534.
- [11] T. Ziegler, *Pure Appl. Chem.* 63 (1991) 873-878.
- [12] J. Andzelm, E. Wimmer, *J. Chem. Phys.* 96 (1992) 1280-1303.
- [13] G.E. Scuseria, *J. Chem. Phys.* 97 (1992) 7528-7530.
- [14] R.M. Dickson, A.D. Becke, *J. Chem. Phys.* 99 (1993) 3898-3905.
- [15] B.G. Johnson, P.M.W. Gill, J.A. Pople, *J. Chem. Phys.* 98 (1993) 5612-5626.
- [16] N. Oliphant, R.J. Bartlett, *J. Chem. Phys.* 100 (1994) 6550-6561.
- [17] M.E. F. Braibante, H.T.S. Braibante, M.P. Uliana, C.C. Costa, M. Spenazzatto, *J. Braz. Chem. Soc.* 19 (2008) 909-913.

- [18] M.M. Mashaly, H.F. El-Shafiy, S.B. El-Maraghy, H.A. Habib, *Spectrochimica Acta A*: 61 (2005) 1853–1869
- [19] G.M. Sheldrick, *Acta Cryst. A: Found. Crystallogr.* 64 (2008) 112-122.
- [20] C.F. Macrae, P.R. Edgington, P. McCabe, E. Pidcock, G.P. Shields, R. Taylor, M. Towler, J. van de Streek, *J. Appl. Cryst.* 39 (2006) 453-457.
- [21] A.L. Spek, Utrecht University, Utrecht, The Netherlands, 20 (2001).
- [22] L.J. Farrugia, *J. Appl. Cryst.* 32 (1999) 837-838.
- [23] M.J. Frisch, G.W. Trucks, H.B. Schlegel, G.E. Scuseria, M.A. Robb, J.R. Cheeseman, J.A. Montgomery Jr., T. Vreven, K.N. Kudin, J.C. Burant, J.M. Millam, S.S. Iyengar, J. Tomasi, V. Barone, B. Mennucci, M. Cossi, G. Scalmani, N. Rega, G.A. Petersson, H. Nakatsuji, M. Hada, M. Ehara, K. Toyota, R. Fukuda, J. Hasegawa, M. Ishida, T. Nakajima, Y. Honda, O. Kitao, H. Nakai, M. Klene, X. Li, J.E. Knox, H.P. Hratchian, J.B. Cross, V. Bakken, C. Adamo, J. Jaramillo, R. Gomperts, R.E. Stratmann, O. Yazyev, A.J. Austin, R. Cammi, C. Pomelli, J.W. Ochterski, P.Y. Ayala, K. Morokuma, G.A. Voth, P. Salvador, J.J. Dannenberg, V.G. Zakrzewski, S. Dapprich, A.D. Daniels, M.C. Strain, O. Farkas, D.K. Malick, A.D. Rabuck, K. Raghavachari, J.B. Foresman, J.V. Ortiz, Q. Cui, A.G. Baboul, S. Clifford, J. Cioslowski, B.B. Stefanov, G. Liu, A. Liashenko, P. Piskorz, I. Komaromi, R.L. Martin, D.J. Fox, T. Keith, M.A. Al-Laham, C.Y. Peng, A. Nanayakkara, M. Challacombe, P.M.W. Gill, B. Johnson, W. Chen, M.W. Wong, C. Gonzalez, J.A. Pople, Gaussian 03, Gaussian, Inc., Wallingford, CT, 2004.
- [24] R. Dennington II, T. Keith, J. Millam, GaussView, Version 4.1.2. Semichem Inc., Shawnee Mission, KS, 2007.
- [25] P.J. Stephens, F.J. Devlin, C.F. Chabalowski, M.J. Frisch, *J. Phys. Chem.* 98 (1994) 11623-11627.
- [26] R. Ditchfield, W.J. Hehre, J.A. Pople, *J. Chem. Phys.* 54 (1971) 724-728.
- [27] S. Miertus, E. Scrocco, J. Tomasi, *Chem. Phys.* 55 (1981) 117-129.
- [28] V. Barone, M. Cossi, *J. Phys. Chem. A* 102 (1998) 1995-2001.

- [29] M. Cossi, N. Rega, G. Scalmani, V. Barone, *J. Comput. Chem.* 24 (2003) 669-681.
- [30] J. Tomasi, B. Mennucci, R. Cammi, *Chem. Rev.* 105 (2005) 2999-3093.
- [31] R. Ditchfield, *J. Chem. Phys.* 56 (1972) 5688-5691.
- [32] Y.X. Sun, Q.L. Hao, W.X. Wei, Z.X. Yu, L.D. Lu, X. Wang, Y.S. Wang, *J. Mol. Struct.* 904 (2009) 74-82.
- [33] C. Andraud, T. Brotin, C. Garcia, F. Pelle, P. Goldner, B. Bigot, A. Collet, *J. Am. Chem. Soc.* 116 (1994) 2094-2102.
- [34] V.M. Geskin, C. Lambert, J.-L. Brédas, *J. Am. Chem. Soc.* 125 (2003) 15651-15658.
- [35] M. Nakano, H. Fujita, M. Takahata, K. Yamaguchi, *J. Am. Chem. Soc.* 124 (2002) 9648-9655.
- [36] D. Sajan, J. Hubert, V.S. Jayakumar, J. Zaleski, *J. Mol. Struct.* 785 (2006) 43-53.
- [37] G. Alpaslan, M. Macit, A. Erdönmez, O. Büyükgüngör, *J. Mol. Struct.* 1016 (2012) 22-29.
- [38] G. Alpaslan, M. Macit, A. Erdönmez, O. Büyükgüngör, *J. Mol. Struct.* 997 (2011) 70-77.
- [39] R.G. Pearson, *Coord. Chem. Rev.* 24 (1994) 401.
- [40] N. Ozbek, G. Kavak, Y. Ozcan, S. Ide, N. Karacan, *J. Mol. Struct.* 919 (2009) 154-159.
- [41] A. Masternak, G. Wenska, J. Milecki, B. Skalski, S. Franzen, *J. Phys. Chem. A* 109 (2005) 759-766.
- [42] Y. Le, J.F. Chen, M. Pu, *Int. J. Pharm. Sci.* 358 (2008) 214-218.
- [43] Z. Zhou, R.G. Parr, *J. Am. Chem. Soc.* 112 (1990) 5720-5724.
- [44] K. Fukui, *Theory of Orientation and Stereoselection*. Springer, Berlin Heidelberg New York (1975).
- [45] I. Fleming, *Frontier Orbital and Organic Chemical Reactions*, John Wiley & Sons, New York (1976).
- [46] N.O. Obi-Egbedi, I.B. Obot, M.I. El-Khaiary, S.A. Umoren, E.E. Ebenso, *Int. J. Electrochem. Sci.* 6 (2011) 5649-5675.
- [47] P. Politzer, P. Lane, *Struct. Chem.* 1 (1990) 159-164.

[48] E. Scrocco, J. Tomasi, Adv. Quantum Chem. 11 (1978) 115-193.

[49] S. Sebastian, N. Sundaraganesan, B. Karthikeyan, V. Srinivasan, Spectrochim. Acta A 78 (2011) 590-600.

[50] S.I. Gorelsky, SWizard Program, Revision 4.5, University of Ottawa, Ottawa, Canada, 2010, <<http://www.sg.chem.net/>>.

ACCEPTED MANUSCRIPT

Highlights

- ▶ Synthesis of triazine heterocyclic derivatives.
- ▶ Molecular geometry of triazine heterocyclic derivative in the ground state using the density functional theory (DFT) with 6-31G(d,p)
- ▶ Crystal structure determination of triazine heterocyclic derivatives

ACCEPTED MANUSCRIPT